Wavelet transform analysis of dynamic speckle patterns texture

Margarita Fernández Limia, Adriana Mavilio Núñez, Héctor Rabal, and Marcelo Trivi

We propose the use of the wavelet transform to characterize the time evolution of dynamic speckle patterns. We describe it by using as an example a method used for the assessment of the drying of paint. Optimal texture features are determined and the time evolution is described in terms of the Mahalanobis distance to the final (dry) state. From the behavior of this distance function, two parameters are defined that characterize the evolution. Because detailed knowledge of the involved dynamics is not required, the methodology could be implemented for other complex or poorly understood dynamic phenomena.

OCIS codes: 100.7410, 030.6140.

1. Introduction

The speckle phenomenon[1] has been extensively used in many applications in nondestructive testing.[2] Dynamic speckle is a related phenomenon occurring when laser light is scattered by objects showing some type of activity.[3,4] This is the case of many biologic samples (seeds, fruits, etc.) and some nonbiological ones, such as corrosion phenomena and the drying of coatings of paint. Several possibilities for the measurement of the activity of the dynamic speckles have already been reported. Namely, the second-order moment of the cooccurrence matrix,[5] the full width at half maximum of the average autocorrelation function,[6,7] the width of equivalent functions that best fit the autocorrelation function,[8] etc. are some examples. In some of them, the time history of the speckle pattern (THSP), as proposed by Oulamara *et al.*[9] is used. These measures are mostly based in estimations of how fast intensity changes in the THSP occur. THSPs depict the time history of the speckle pattern as images. These images show different textures for different phenomena or different states of the same phenomenon. It can be reasonably expected that techniques that are useful to characterize textures could also be used to characterize the underlying state of the sample. Therefore an approach to characterize the time evolution of these dynamic speckle patterns could be provided by textural analysis of THSP images of the process evolution. Many methods for texture analysis have been reported,[10,11] such as statistical and spectral ones using digital filtering.[12,13] One of the most current and advantageous is that using multiresolution analysis by employing the wavelet transform (WT).[14,15] Multiresolution representations are very effective for analyzing the information content of images.

In this work, we develop a methodology to characterize the evolution of the THSP using the WT. One of the aims of this work is to find optimal texture features for this task. The time evolution of the speckle patterns is described through the behavior of the Mahalanobis distance function.[15,16] This distance is calculated between texture features of the THSP corresponding to different stages of a phenomenon and the same features of, for example, the lowest activity THSP. Parameters are then defined that make possible the characterization of the time evolution.

As an illustrative example, the WT technique is described here as is applied to the assessment of the drying of synthetic paint in different stages of the process. That process has already been studied by using alternative speckle methods.[17]

As this procedure involves a supervised learning step, the paint can be nonetheless adapted to the

M. F. Limia and A. M. Núñez are with the Departamento de Física, Instituto Superior Politécnico "José A. Echeverría", Facultad de Ingeniería Eléctrica, Calle 127 s/n, Apartado 6028, Marianao 15, La Habana, Cuba. H. Rabal and M. Trivi are with the Centro de Investigaciones Ópticas (CIC-CONICET) and UID Optimo, Departamento de Fisicomatemáticas, Facultad de Ingeniería, Universidad Nacional de La Plata, Casilla de Correo 124, 1900 La Plata, Argentina.

Received 21 March 2002; revised manuscript received 23 July 2002.

0003-6935/02/326745-06$15.00/0

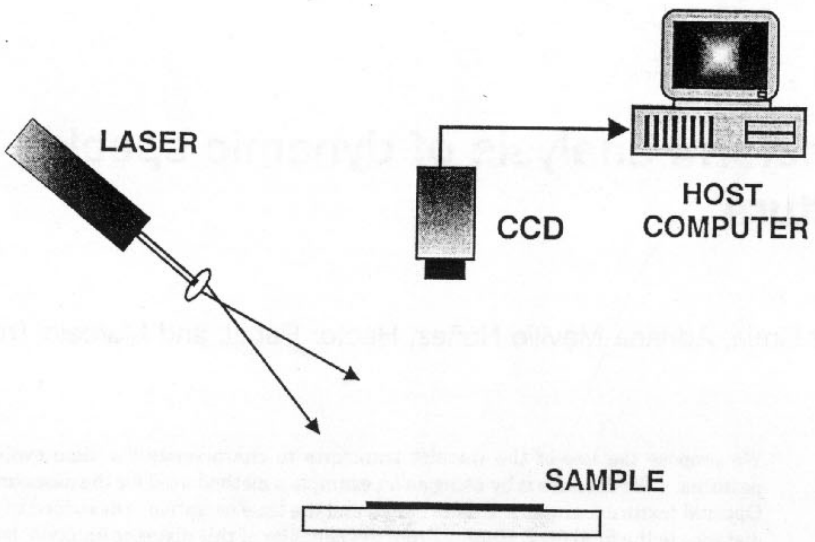

Fig. 1. Experimental setup.

followup of other phenomena without requiring a precise knowledge of its dynamics.

2. Time-History Images of Dynamic Speckle Patterns

In the experiments, dynamic speckle patterns that correspond to different drying stages in samples of synthetic paint were registered after extending it on a glass surface by means of an extender.

The experimental setup is shown in Fig. 1. The samples were illuminated with an expanded and attenuated 10 mW He–Ne laser. The free-propagation speckle-pattern images were then registered by a CCD camera, digitized to eight bits by a frame grabber and stored in the memory of a personal computer. Care was taken so that the size of the speckles was well resolved by the CCD sensor.

To show the time evolution of a speckle pattern we used the Oulamara *et al.* method.[9] We registered 512 successive images of the dynamical speckle pattern for every state of the phenomenon being assessed. A certain column, usually the middle one, was then selected in each of them. With the selected column set, a new 512 × 512 pixel composite image was then constructed. In this image, named the THSP, the rows represent different points on the object and the columns represent their intensity state in every sampled instant. The activity of the sample appears as the intensity changes in the horizontal direction. When the phenomenon is very active (wet paint), the THSP resembles an ordinary (spatial) speckle pattern as shown in Fig. 2(a). Conversely, when a phenomenon shows low activity (dry paint), time variations of the speckle pattern are slow and the THSP shows an elongated shape [see Fig. 2(c)]. An intermediate drying state THSP is also shown [Figure 2(b)]. Different textures can be seen in these images that are characteristic of each drying state. It is to these textures that the WT method is going to be applied.

The time interval between the acquisition of consecutive columns in a THSP is 0.08 s and for the construction of a full THSP image it is 40 s. The sampling interval or time interval between two (considered) consecutive drying stages was 4 min. We

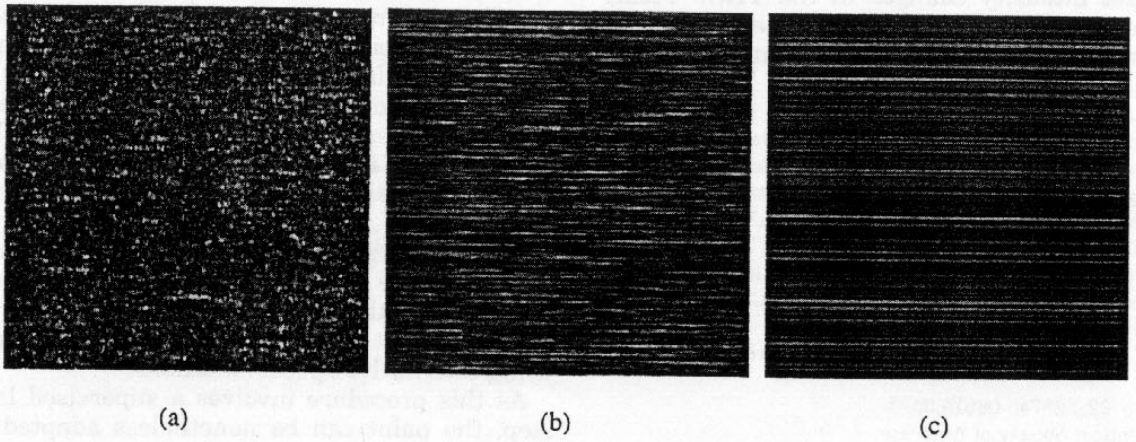

Fig. 2. THSP corresponding to three different drying stages: (a) wet paint, (b) intermediate state of drying, (c) dry paint.

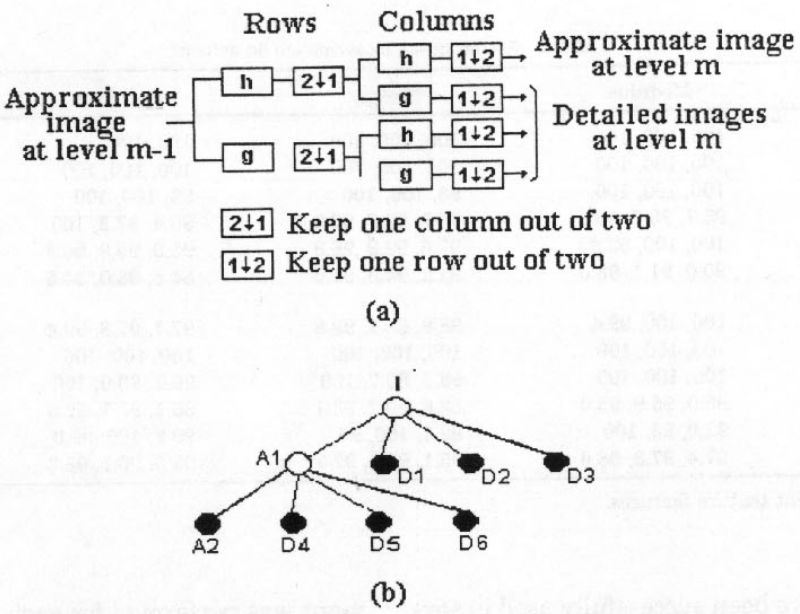

Fig. 3. (a) Hierarchical decomposition of an image, (b) pyramidal wavelet decomposition.

assume that each drying stage can be characterized by the textures of the corresponding THSP image. Fourteen different drying stages (14 THSP images) were considered as texture patterns.

3. Wavelet Transform Method

The WT uses a family of wavelet functions and its associated scaling functions to develop the original image $I(x, y)$ in different frequency subbands. The decomposition procedure is successively applied to the lowest frequency subband to obtain the next level of decomposition. The wavelet filters $\{g\}$ (bandpass) and scaling $\{h\}$ (lowpass) are applied in both horizontal and vertical directions followed by a two-to-one subsampling in the image.

The results are three detailed images $[D^k{}_l I(x, y)]$ $k = 1, 2, 3$ containing high frequencies in the horizontal direction, in the vertical direction, or both respectively, depending on the selected orientation; and one approximate $[A_l I(x, y)]$ that corresponds to the lowest frequency subband, both in the horizontal and in the vertical directions. Here l denotes the decomposition level or resolution. The procedure is then repeated on the approximate image to obtain the next resolution level (see Fig. 3).

In this work, $I(x, y)$ are the pixel-intensity values of the THSPs.

Texture Feature Vectors. Texture features are calculated from the coefficients c_{ij} of the development of the image $I(x, y)$ in the selected wavelet basis. The index i indicates the terminal frequency channel or subband, and j takes M values. M is the number of coefficients associated with the subband i. The features: modulus, energy, standard deviation, and average residual were calculated for every terminal frequency channel i by using the expressions

$$md_i = \frac{1}{M}\sum_{j=1}^{M} |c_{i,j}|, \tag{1}$$

$$E_i = \frac{1}{M}\sum_{j=1}^{M} |c_{i,j}|^2, \tag{2}$$

$$sd_i = \left(\sum_{j=1}^{M} \frac{(c_{i,j} - vm_i)^2}{M-1}\right)^{1/2}, \tag{3}$$

$$\mathrm{rms}_i = \frac{1}{M}\sum_{j=1}^{M} |c_{i,j} - vm_i|, \tag{4}$$

where vm_i is the mean value of the M coefficients of the frequency channel i.

The feature vectors are conformed by taking as vector components the values of the features corresponding to the terminal frequency channels.

Spatial frequency is related to texture because fine textures are rich in high spatial frequencies while coarse textures are rich in low spatial frequencies. Therefore the values of the decomposition coefficients and their distribution in the different frequency channels bear textural information of the image. Consequently, the feature vectors that are calculated based on this distribution should also carry this textural information.

4. Numerical Experiment

A numerical experiment was carried out to select the optimal texture feature and the appropriate wavelet basis. In particular, the compactly supported orthogonal wavelet bases: Haar, Daubechies-2, and Daubechies-8 were used, because the orthogonal

Table 1. Results of the classification (in percent)[a]

Image/Feature	Modulus	Energy	Std. Dev.	Ave. Residual
Lat 3	100, 100, 100	100, 100, 100	100, 100	100, 100, 100
Lat 4	100, 100, 100	100, 100, 100	100, 100, 100	100, 100, 100
Lat 5	100, 100, 100	98, 100, 100	99, 100, 100	100, 100, 100
Lat 6	95.7, 93.7, 99.5	88.2, 85.7, 97.9	90.4, 87.2, 100	96.8, 93.7, 100
Lat 7	100, 100, 92.9	97.6, 99.9, 96.8	95.9, 99.9, 96.6	100, 100, 97.0
Lat 8	90.0, 91.1, 98.0	82.2, 94.5, 91.6	84.8, 93.0, 94.5	91.8, 90.7, 98.1
Lat 9	100, 100, 99.4	98.8, 98.1, 99.8	97.7, 97.8, 99.4	97.1, 99.4, 96.9
Lat 10	100, 100, 100	100, 100, 100	100, 100, 100	100, 100, 100
Lat 12	100, 100, 100	98.5, 89.7, 100	99.2, 90.0, 100	100, 100, 100
Lat 13	93.0, 95.9, 95.0	83.6, 90.3, 93.1	85.1, 90.1, 92.5	92.6, 96.9, 93.3
Lat 14	92.0, 95, 100	99.3, 100, 96	99.2, 100, 99.0	98.6, 100, 97.0
Total	97.4, 97.8, 98.6	95.1, 96.2, 97.7	95.5, 96.1, 98.3	97.9, 98.2, 98.3

[a]When using the different texture features.

Daubechies bases have been successfully used in several works related to the texture analysis of images,[14,15,18] and the Haar basis is the simplest one.

As speckles in the THSPs are spatially well resolved (that is, speckle grains sometimes occupy more than one pixel in the space direction) the consecutive rows of the THSP are partially correlated. So, two-dimensional wavelets were used.

Pattern Construction. The feature vectors corresponding to each of the 14 THSP images (texture patterns) were constructed. The steps indicated next were followed:

Each THSP image of the size (512 × 512) pixel was histogram equalized to obtain textures with approximately the same first-order statistics.

- A set of 25 image samples of 256 × 256 pixels^2 were extracted from each THSP image. This set was representative of all the regions of the corresponding THSP image. These images were extracted in order considering that new elements were always present, so that the set was representative of the whole THSP image.
- The wavelet decomposition of each image sample was then performed up to decomposition level $N = 2$ reaching finally to 7 terminal frequency subbands.
- For each image sample the values of the features [Eqs. (1–4)] were determined for every one of the seven terminal-frequency channels. These values were averaged on the set of the 25 image samples corresponding to a THSP image and then the representative feature seventh-dimension vectors or texture-pattern vectors were conformed. The covariance matrix cov_{tf} was also calculated for each feature vector $f = 1, \ldots, 4$ and for each texture pattern $t = 1, \ldots 14$.

This procedure was performed by using each of the mentioned orthogonal wavelet bases.

Classification. The following classification experiment was performed for each texture feature and by using each of the mentioned orthogonal wavelet bases:

- Another set of 100 image samples was randomly extracted from each THSP image corresponding to each drying stage.
- Each image sample was decomposed up to a level $N = 2$. The feature vectors were determined for each image sample.
- The Mahalanobis distances between the sample feature vector ($\mathbf{u}_f$) ($f = 1 \ldots 4$) and the feature vectors ($\mathbf{u}_{tf}$) of the 14 texture patterns were then computed by means of the formula[15,16]:

$$D_{tf} = (\mathbf{u}_f - \mathbf{u}_{tf})^T \mathrm{cov}_{tf}^{-1} (\mathbf{u}_f - \mathbf{u}_{tf}) \quad (5)$$

- The texture class corresponding to the smallest distance was assigned to the image sample.

The optimal features were selected taking into account the greatest percentage of correct classifications for each used wavelet basis.

The features that showed better discrimination were the modulus and the mean residual, as can be seen in Table 1. This could be concluded from these results that show that the percentages of correct classifications for these features were always greater than 90%. Besides, the wrong classifications in the case of these features only involved confusions for a small number of textures, and it only happened with the time-nearest ones. This was not so with the features of energy and standard deviation. In what follows, the modulus and the average residual will be the only considered features.

In a general sense, the results of the classification experiment for the selected features did not show significant differences for the used wavelet bases.

5. Time Evolution Characterization of the Drying Process

Owing to the random fluctuations of the image texture in each stage of drying, a set of 10 different

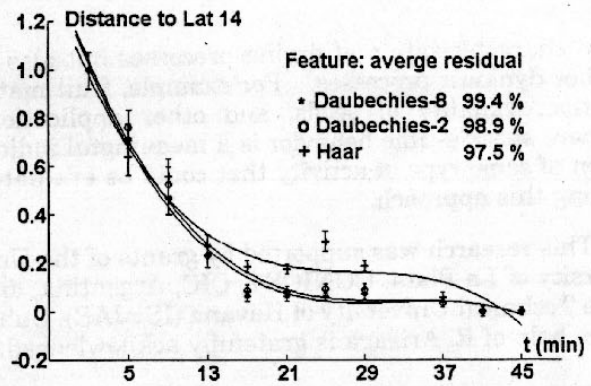

Fig. 4. Behavior of the distance function to Lat 14 calculated for the average residual feature by using the orthogonal bases Daubechie-8 (asterisks), Daubechies-2 (open circles), and Haar (crosses). The percentages represent the third-degree polynomial fit quality.

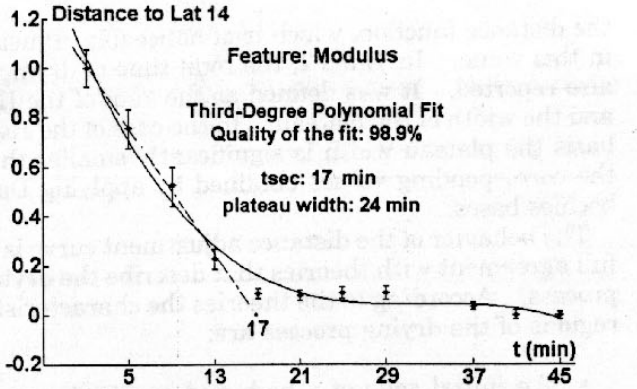

Fig. 5. Behavior of the distance function to Lat 14 calculated for the modulus feature by using the Daubechies-2 basis. The solid curve represents a third-degree polynomial fit. The straight line (dashed), corresponds to the linear fit of the first experimental points.

realizations of the feature vectors for each THSP image was performed by following the steps described in the *Pattern Construction* Subsection.

To characterize the time evolution of the drying process, the Mahalanobis distance was calculated between each texture pattern to be $t = 1, \ldots, 13$ and that corresponding to the THSP with lowest activity $t = 14$. This distance was calculated for the 10 mentioned realizations, and the obtained values were averaged. The calculations were done for each of the mentioned wavelet bases and for the two selected features. Figure 4 shows the behavior of the Mahalanobis distance for the feature average residual over time by use of the mentioned wavelet bases. In all cases an almost linear steep descent is observed in the initial region of the curve. Then a plateau-like or slow-variation region appears that finally falls to zero. The experimental points were adjusted to a third-degree polynomial. The best quality that resulted from the adjustment was obtained in the case of the Daubechies-8 basis and it is evident that the results obtained with the Haar decomposition can not be optimally fitted with a third-order polynomial expansion.

Although the values of the features modulus and average residual gave very different results, the distances obtained and the parameters of the adjustment curves for both features were very similar. So, they can be used indiscriminantly.

Figure 5 shows the distance function to Lat 14 pattern ($t = 14$) calculated by using the feature modulus with the Daubechies-2 (db-2) basis. A very similar result is obtained for the case by using Daubechies-8 (db-8).

Taking into account the experimental values of the distance in Fig. 5, the value of the time instant T_0 when a sudden change in slope occurs was numerically determined. Then, a linear adjustment with the points before T_0 was performed. The time axis intercept of the adjustment straight line provides a parameter that characterizes how fast the initial drying stage (IDT) is. After the constant rate period, a region can be observed where the slope of the distance adjustment curve falls until a plateau region is reached.

Another interesting parameter for this process is the temporal width of this plateau region. It was calculated by locating the inflection point of the adjustment curve and assuming that it is located at the center of the plateau.

In Table 2, the values of the mentioned parameters are shown for the three wavelet bases and for the two selected features. The obtained values of the distance function were adjusted, in one case to a third-order polynomial and in the other case to a polynomial of the fifth degree. Concerning the parameter IDT, there are not noticeable differences. That is not the case concerning the width of the plateau. The value of this parameter depends on the fitting polynomial degree. As could be expected, the determination of the width of the plateau is more precise in the case of the adjustment with a fifth-order polynomial, because it allows a better description of the behavior of the final region of

Table 2. Drying Parameters

	Mod.			Ave. Res.		
Parameters/Basis	db-8	db-2	Haar	db-8	db-2	Haar
IDT	17.8/17.8	17/17	17/17	17.8/17.8	17/17	17/17
Plateau width	24/15	24/15	17.8/9.7	24.4/15	24.4/15	18.2/9.7
Drying time	41.8/32.8	41/32	34.8/26.7	42.2/32.8	41.4/32	35.2/26.7

[a]In min.

the distance function, which is of noticeable influence in this value. In Table 2, the total time of drying is also reported. It was defined as the sum of the IDT and the width of the plateau. In the case of the Haar basis the plateau width is significantly smaller than the corresponding values obtained by applying Daubechies bases.

The behavior of the distance adjustment curve is in full agreement with theories that describe the drying process. According to the theories the characteristic regions of the drying process are:

- An initial zone of a high and constant rate of change,
- A second zone where the rate of change is slower,
- A third zone (plateau) where the rate of change is a minimum.

In theories of drying of coatings,[17] the initial stage of the process is called the constant-rate period. After this constant-rate period, there is a falling-rate period in which the drying rate decreases to zero. The falling-rate period is believed to be the result of slower diffusion of a solvent through a dry surface layer after the surface of the solvent–air interface recedes from the surface. The starting time of the falling-rate period depends on the film thickness and solvent evaporation.

6. Conclusions

We report a method of analysis to characterize the phenomenon of dynamic speckle by using the wavelet transform. As an example, it is applied to the study of the time evolution of the drying of synthetic paint. Starting with a numerical experiment, a methodology is proposed to process dynamic speckle patterns. Two parameters are defined, the initial drying time and the width of the plateau. These parameters allow the characterization of the drying process, and consequently they can be used for quality control in the production of this type of paint and to compare different types of paint.

The numerical experiment demonstrated that the recommended methodology is valid for any one of the applied wavelet bases. It also showed that the texture features: modulus and average residual, calculated from the wavelet expansion coefficients, are appropriate for this task. No significant differences between them were observed, independently of the wavelet basis used.

The obtained results for the proposed example are similar to those obtained before with other speckle methods (see Ref. 17). Nevertheless, this approach is based on the comparison of textures instead of the estimation of an activity measurement. Situations can be imagined where different textures give similar activity measurements and conversely, where similar textures give different activity measurements. So a direct comparison between this new approach and the already existing activity measures is not appropriate.

The proposed method could be of use, not only for the characterization of drying processes but also to other dynamic processes. For example, fruit maturation, viability of seeds, and other applications where speckle-time behavior is a meaningful indication of some type of activity that could be evaluated using this approach.

This research was supported by grants of the University of La Plata, CONICET, CIC, Argentina, and the Technical University of Havana (ISPJAE), Cuba. The help of R. Arizaga is gratefully acknowledged.

References and Note

1. J. C. Dainty, *Laser Speckle and Related Phenomena*, (Springer-Verlag, Berlin, 1975).
2. R. S. Sirohi, ed., *Speckle Metrology*, (Marcel Dekker, New York, 1993).
3. Y. Aizu and T. Asakura, "Biospeckle," *Trends in Optics*, A. Consortini, ed. (Academic, San Diego, 1996), Chap. 2.
4. H. J. Rabal, M. Trivi, R. Arizaga, G. Romero, and E. Alanis, "Transient phenomena analysis using dynamic speckle patterns," Opt. Eng. **35**, 57–60 (1996).
5. R. Arizaga, M. Trivi, H. J. Rabal, "Speckle time evolution characterization by the cooccurrence matrix analysis," Opt. Laser Technol. **31**, 163–169 (1999).
6. Y. Aizu and T. Asakura, "Bio-speckle phenomena and their applications to the evaluation of blood flow," Opt. Laser Technol. **23**, 205–219 (1991).
7. G. J. Tearney and B. E. Bouma, "Atherosclerotic plaque characterization by spatial and temporal speckle pattern analysis," Opt. Lett. **27**, 533–535 (2002).
8. G. Romero, E. Alanis, and H. J. Rabal, "Statistics of the dynamic speckle produced by a rotating diffuser and its applications to the assessment of paint drying," Opt. Eng. **39**, 1652–1658 (2000).
9. A. Oulamara, G. Tribillon, and J. Doubernoy, "Biological activity measurements on botanical specimen surfaces using a temporal decorrelation effect of laser speckle," J. Mod. Opt. **36**, 165–179 (1989).
10. R. Haralick, "Statistical and Structural Approaches to Texture," Proc. IEEE **67**, 786–803 (1979).
11. M. Unser, "Sum and difference histograms for texture classification," IEEE Trans. Pattern Anal. Mach. Intell. PAMI **8**, 118–125 (1986).
12. M. Tejera, A. Mavilio, and M. Fernández, "Dimensiones promediadas como descriptores de textura," presented at Foro Iberoam. Trat. Dig. Imag. y Visión Industrial, Valencia, Spain, 5–8 Oct. 1996.
13. T. P. Weldon and W. E. Higgins, "Design of multiple Gabor filters for texture segmentation," in IEEE Trans. Acoust. Speech, Signal Proc. (ICASSP96) IV, Atlanta, Ga., 2245–2248 (1996).
14. M. Fernández, A. Mavilio, and M. Tejera, "Texture segmentation of a 3D seismic section with wavelet transform and Gabor filters," in *Proceeding of the IEEE of the 15th International Conference on Pattern Recognition*, **3**, 358–361 (2000).
15. T. Chang and C. C. J. Kuo, "Texture Analysis and Classification with Tree-Structured Wavelet Transform," IEEE Trans. Image Process. **2**, 429–441 (1993).
16. See, for example, R. O. Duda http://www.engr.sjsu.edu/~knapp/HCIRODPR/PR_home.htm.
17. J. Amalvy, C. Lasquibar, R. Arizaga, H. Rabal, and M. Trivi, "Application of dynamic speckle interferometry to the drying of coatings," Progress in Organic Coatings **42**, 89–99 (2001).
18. V. Manian and R. Vasquez, "Scaled and rotated texture segmentation using a class of basis functions," in *Wavelet Applications IV*, H. H. Szu, ed., Proc. SPIE **3078**, 324–332 (1997).